

RSC Advances



This is an *Accepted Manuscript*, which has been through the Royal Society of Chemistry peer review process and has been accepted for publication.

Accepted Manuscripts are published online shortly after acceptance, before technical editing, formatting and proof reading. Using this free service, authors can make their results available to the community, in citable form, before we publish the edited article. This *Accepted Manuscript* will be replaced by the edited, formatted and paginated article as soon as this is available.

You can find more information about *Accepted Manuscripts* in the [Information for Authors](#).

Please note that technical editing may introduce minor changes to the text and/or graphics, which may alter content. The journal's standard [Terms & Conditions](#) and the [Ethical guidelines](#) still apply. In no event shall the Royal Society of Chemistry be held responsible for any errors or omissions in this *Accepted Manuscript* or any consequences arising from the use of any information it contains.

Electronic structure and thermoelectric properties of Zintl compounds $\text{Sr}_5\text{Al}_2\text{Sb}_6$ and $\text{Ca}_5\text{Al}_2\text{Sb}_6$: First-principles study

Lingyun Ye, Yuan Xu Wang^a, Jueming Yang, Yuli Yan, Jihua Zhang, Libin Guo, and Zhenzhen Feng
*Institute for Computational Materials Science,
School of Physics and Electronics, Henan University,
Kaifeng 475004, People's Republic of China*

(Dated: May 5, 2015)

Abstract

Previous experimental work showed that Zn-doping only slightly increased the carrier concentration of $\text{Sr}_5\text{Al}_2\text{Sb}_6$ and the electrical conductivity improved weakly, which is very different from Zn-doping in $\text{Ca}_5\text{Al}_2\text{Sb}_6$. To understand their different thermoelectric behavior, we investigated their stability, electronic structure, and thermoelectric properties by using first-principles calculations and the semiclassical Boltzmann theory. We found that the low carrier concentration of Zn-doped $\text{Sr}_5\text{Al}_2\text{Sb}_6$ mainly come from its high positive formation energy. Moreover, we predict that the high hole concentration can be possibly realized in $\text{Sr}_5\text{Al}_2\text{Sb}_6$ by Na or Mn doping, due to the negative and low formation energies of Na- and Mn-doped $\text{Sr}_5\text{Al}_2\text{Sb}_6$, especially for Mn doping (-6.58 eV). For *p*-type $\text{Sr}_5\text{Al}_2\text{Sb}_6$, the large effective mass along Γ -Y induces a large Seebeck coefficient along the *y* direction, which leads to the good thermoelectric properties along the *y* direction. For *p*-type $\text{Ca}_5\text{Al}_2\text{Sb}_6$, the effective mass along Γ -Z is always smaller than those along other two directions with increasing of doping degree, which induces its good thermoelectric properties along the *z* direction. The analysis of the weight mobility of the two compounds confirms this idea. The calculated band structure shows that $\text{Sr}_5\text{Al}_2\text{Sb}_6$ has a larger band gap than $\text{Ca}_5\text{Al}_2\text{Sb}_6$. The relative small band gap of $\text{Ca}_5\text{Al}_2\text{Sb}_6$ mainly results from the appearing of a high density-of-states peak around the conduction band bottom, which is originated from the Sb-Sb antibonding states in it.

^a Email: wangyx@henu.edu.cn

I. INTRODUCTION

The thermoelectric energy conversion technology has attracted great attention in the past few years, due to its great potential in averting a global energy crisis. However, the widespread application of the conversion technology is limited by the relative low efficiency of current thermoelectric materials, which is characterized by its figure of merit, $ZT = S^2\sigma T/\kappa$, where S is the thermopower or Seebeck coefficient, T is the absolute temperature, σ is the electrical conductivity, and κ is the thermal conductivity.[1] Obviously, an ideal thermoelectric material requires a large Seebeck coefficient, a high electrical conductivity, and a low thermal conductivity. However, S and σ oppositely depend on carrier concentration.[2] Thus, it is difficult to obtain large S and σ simultaneously. With the increasing of carrier concentration, the Seebeck coefficient decreases, while the electrical conductivity increases.

Zintl compounds, characterized by covalently bonded anionic substructures which surrounded by cations, have been suggested to be promising thermoelectric materials and attracted great attention. In Zintl compounds, cations donate their electrons to electronegative anions. As a result of the combination of ionic bonding and covalent bonding, Zintl compounds have complex crystal structure with large unit cell, and exhibit ‘electron crystal-phonon glass’ behavior.[3–5] Good thermoelectric performance is often found in doped semiconductors with carrier concentrations from 10^{19} cm^{-3} to 10^{21} cm^{-3} . [2] Because the Seebeck coefficient and the electrical conductivity oppositely depend on the carrier concentration, it is necessary to find an optimal carrier concentration to increase the thermoelectric power factor.

$\text{Sr}_5\text{Al}_2\text{Sb}_6$ has been experimentally synthesized and was found to be a valence-precise Zintl phase compound.[6] It has a similar crystal structure with $\text{Ca}_5\text{Al}_2\text{Sb}_6$ which has been proved to be a promising thermoelectric material.[7–9] $\text{Ca}_5\text{Al}_2\text{Sb}_6$ is composed of infinite corner-sharing MSb_4 tetrahedra chains, and the chains connect to adjacent ones via covalent Sb-Sb bonds forming a ladders-like structure. $\text{Sr}_5\text{Al}_2\text{Sb}_6$ is also composed of corner- and edge-sharing MSb_4 tetrahedra chains, but the chains are non-linear and oscillate. Moreover, previous experimental work shows that $\text{Sr}_5\text{Al}_2\text{Sb}_6$ has a lower thermal conductivity (0.53 W/mK) [6] than $\text{Ca}_5\text{Al}_2\text{Sb}_6$ (0.70 W/mK[7]) at 800K. The experimental ZT value of undoped $\text{Sr}_5\text{Al}_2\text{Sb}_6$ is only 0.05 at 800 K, due to its low carrier concentration and intrinsic electronic properties.[6] The similarity and difference between $\text{Sr}_5\text{Al}_2\text{Sb}_6$ and $\text{Ca}_5\text{Al}_2\text{Sb}_6$ motivate the

current study of $\text{Sr}_5\text{Al}_2\text{Sb}_6$.

Previous studies have shown that doping may improve the figure of merit of thermoelectric materials by optimizing their carrier concentration.[7, 8, 10–12] To find an optimal carrier concentration for $\text{Sr}_5\text{Al}_2\text{Sb}_6$, we studied its electronic structure and thermoelectric properties in this work. The dependence of the Seebeck coefficient, the electrical conductivity, and ZT values on carrier concentration was investigated by the semiclassical Boltzmann theory. Moreover, previous experimental works show that the electrical conductivity of Zn-doped $\text{Sr}_5\text{Al}_2\text{Sb}_6$ is much smaller than that of Zn-doped $\text{Ca}_5\text{Al}_2\text{Sb}_6$, which mainly come from the relative low carrier concentration of Zn-doped $\text{Sr}_5\text{Al}_2\text{Sb}_6$. Therefore, it is valuable to explore the reason for the low carrier concentration of Zn-doped $\text{Sr}_5\text{Al}_2\text{Sb}_6$. We studied the effect of different elements doping on stability of $\text{Sr}_5\text{Al}_2\text{Sb}_6$ by calculating their formation energy. It is found that the formation energy of Zn-doped $\text{Sr}_5\text{Al}_2\text{Sb}_6$ is very high, indicating the low solubility of Zn doping in $\text{Sr}_5\text{Al}_2\text{Sb}_6$. Na and Mn doping are suggested as good candidates for *p-type* doping to improve the thermoelectric performance of $\text{Sr}_5\text{Al}_2\text{Sb}_6$. It is found that the ZT value of $\text{Sr}_5\text{Al}_2\text{Sb}_6$ can be largely increased by tuning its carrier concentration.

II. COMPUTATIONAL DETAIL

The structure of $\text{Sr}_5\text{Al}_2\text{Sb}_6$ was optimized with the Vienna *ab initio* simulation package (VASP) which based on density functional theory (DFT).[13, 14] The exchange-correlation potential was in the form of Perdew-Burke-Ernzerhof (PBE) generalized-gradient approximation (GGA). The plane-wave cutoff energy was set to be 500 eV, and for the Brillouin-Zone integration, a $4 \times 5 \times 4$ Monkhorst-Pack special k-points grid was used. The energy convergence criterion was chosen to be 10^{-6} eV. The Hellmann-Feynman forces on each ion were less than 0.02 eV/Å.

The electronic structure of $\text{Sr}_5\text{Al}_2\text{Sb}_6$ was calculated with the full-potential linearized augmented plane waves method[15] which implemented in WIEN2k.[16–18] We also calculated the forces on each atom by using WIEN2k and found that the forces on each atom are smaller than 0.02 eV/Å, and the calculated forces are listed in Table S1, ESI. Here, the PBE-GGA was used as the exchange-correlation potentials, and the cutoff parameter, $R_{mt}K_{max} = 7$ (K_{max} is the magnitude of the largest \mathbf{k} vector and R_{mt} is the smallest muffin-tin radius), controls the basis-set convergence. The muffin-tin radii were 2.5 a.u. for Sr,

Al, and Sb atoms. Self-consistent calculations were performed with 120 k-points in the irreducible Brillouin zone, and the total energy was converged when the energy difference was less than 0.0001 Ry.

The transport properties of $\text{Sr}_5\text{Al}_2\text{Sb}_6$ were evaluated by the semiclassical Boltzmann theory, with the constant scattering time approximation implemented in the Boltz-Trap code.[19] This approximation is based on a smoothed Fourier interpolation of the bands, and is often applied for metals and degenerately doped semiconductors. In this method, it is supposed that the scattering time determining electrical conductivity does not vary strongly with energy on the scale of kT . It also assumes that the band structure near band gap does not change with the different doping level, that is to say the carrier concentration just changes the situation of the chemical potential. In this work, the calculated band gap of $\text{Sr}_5\text{Al}_2\text{Sb}_6$ was approximately 0.78 eV, which is agreement with the previous experimental value.[6]

III. RESULTS AND DISCUSSIONS

A. Crystal structure and formation energy

$\text{Sr}_5\text{Al}_2\text{Sb}_6$ is orthorhombic with space group of $Pnma$. Each primitive cell contains 52 atoms, and there are two, five, and two crystallographically unique Sr, Sb, and Al atoms, as shown in Table I. The optimized $\text{Sr}_5\text{Al}_2\text{Sb}_6$ lattice constants are $a = 11.9270 \text{ \AA}$, $b = 10.2246 \text{ \AA}$, and $c = 13.1086 \text{ \AA}$. Fig. 1 shows the optimized crystal structure of $\text{Sr}_5\text{Al}_2\text{Sb}_6$. For comparison, the crystal structure of $\text{Ca}_5\text{Al}_2\text{Sb}_6$ is shown in Fig. 2. As seen in Fig. 1, $\text{Sr}_5\text{Al}_2\text{Sb}_6$ is composed of infinite chains, which are formed from corner and edge sharing AlSb_4 tetrahedra and extend along the a -axis, and the chains oscillate back and forth along c -axis. The Sr atoms are situated between tetrahedral chains to provide overall charge balance. A primitive cell of $\text{Ca}_5\text{Al}_2\text{Sb}_6$ contains 26 atoms, and the simple ladder-like chains are composed of corner sharing AlSb_4 tetrahedra. The different structures of $\text{Ca}_5\text{Al}_2\text{Sb}_6$ and $\text{Sr}_5\text{Al}_2\text{Sb}_6$ may result from the combination of relatively large cation (Sr) and a small triel element (Al) in $\text{Sr}_5\text{Al}_2\text{Sb}_6$. [6] Within the Zintl formalism, the valence balance of $\text{Sr}_5\text{Al}_2\text{Sb}_6$ can be understood as follows: each tetrahedrally coordinated aluminium atom has a formal valence of -1, due to being bound to four antimony atoms; the two edge sharing Sb1 atoms, one corner sharing

Sb3 atoms, and the Sb2 atoms have two bonds and can be considered to have a valence of -1; Sb4 and Sb5 are singly-bonded to Al and Sb2 atoms respectively, thus their valence can be considered as -1. The anionic unit can thus be written as $[(Al^{-1})_2(Sb^{-2})_2(Sb^{-1})_4]$. Sr^{+2} ions situate between the chains and provide overall charge balance. Therefore, $Sr_5Al_2Sb_6$ can be expressed as $Sr_5^{+2}Al_2^{-1}Sb_2^{-2}Sb_4^{-1}$.

Previous experimental work has shown that the relative low carrier concentration of $Sr_5Al_2Sb_6$ leads to its low electrical conductivity, which induced its low thermoelectric performance.[6] Zevalkink et al. tried to increase the hole concentration of $Sr_5Al_2Sb_6$ by Zn^{2+} doping on Al^{3+} site. [6] However, the measured carrier concentration of the Zn-doped sample is only slightly higher than that of the undoped sample, suggesting that the attempt to substitute Zn^{2+} on the Al^{3+} site is unsuccessful. This phenomenon can be explained by the formation energy of Zn-doped $Sr_5Al_2Sb_6$. Inspired by previously studies[7, 20] of $Ca_5Al_2Sb_6$ doped with Na^{1+} at Sr^{2+} site and Mn^{2+} at Al^{3+} site, it is believed that different elements doping should be tried to increasing the hole carrier concentration of $Sr_5Al_2Sb_6$. In the current work, we calculated the formation energy of $Sr_5Al_2Sb_6$ with different dopant. The formation energy was estimated from the following:

$$E_f = E_{doped} - E_{undoped} - E_A + E_B, \quad (1)$$

where E_{doped} and $E_{undoped}$ are the total energies of $Sr_5Al_2Sb_6$ with and without doping at their most stable states, respectively. E_A and E_B are energies of dopant atom and host atom. Here, only one host atom is substituted by a dopant atom, thus the doping level for Na^{1+} or K^{1+} at Sr^{2+} site is 0.125, and Zn^{2+} or Mn^{2+} at Al^{3+} site is 0.05. The calculated formation energies are listed in Table III. It is important to point out that the formation energy of the Zn-doped $Sr_5Al_2Sb_6$ is 15.80 eV, suggesting that Zn-doping is difficult to increase the hole carrier concentration and the low solubility of Zn in $Sr_5Al_2Sb_6$. This is in agreement with the experimental result perfectly.[6] The calculated formation energies of the K-doped and Na-doped in the Sr site are 5.20 eV and -3.32 eV, respectively, meaning that the stability of Na-doped $Sr_5Al_2Sb_6$ is stronger than that of K-doped. Thus, Na-doped $Sr_5Al_2Sb_6$ may be easier to be realized and have higher hole concentrations. The possible reason is the smaller atomic radius of Na than that of K. The calculated formation energy of Mn-doped on the Al site are negative: -6.58 eV, which suggests that Mn doping may be easier to be realized and have higher hole concentrations in $Sr_5Al_2Sb_6$. Thus, we can predict that the doped

$\text{Sr}_5\text{Al}_2\text{Sb}_6$ with Na^{1+} at the Sr^{2+} site and Mn^{2+} at the Al^{3+} site may be synthesized and have high hole carrier concentrations, and they correspond to p -type doping.

B. Electronic structure

$\text{Sr}_5\text{Al}_2\text{Sb}_6$ has the different crystal structure from $\text{Ca}_5\text{Al}_2\text{Sb}_6$, which leads to their different electronic structures. Because the transport properties of materials are predominantly affected by the electronic structure near the Fermi level, it is reasonable to focus discussion on the feature of the valence band maximum (VBM) and the conduction band minimum (CBM). Fig. 3 shows the calculated band structure of $\text{Sr}_5\text{Al}_2\text{Sb}_6$ and $\text{Ca}_5\text{Al}_2\text{Sb}_6$. As seen in this figure, $\text{Sr}_5\text{Al}_2\text{Sb}_6$ is a semiconductor with an indirect band gap of 0.78 eV. The VBM of $\text{Sr}_5\text{Al}_2\text{Sb}_6$ is located at Γ point, and the CBM is located between Z and Γ points. $\text{Ca}_5\text{Al}_2\text{Sb}_6$ is a direct band gap semiconductor with a band gap of 0.53 eV. The VBM and CBM of $\text{Ca}_5\text{Al}_2\text{Sb}_6$ are both located at Γ point. Comparing the band structures of $\text{Sr}_5\text{Al}_2\text{Sb}_6$ and $\text{Ca}_5\text{Al}_2\text{Sb}_6$, it is obviously found that the dispersion of the VBM and CBM of $\text{Sr}_5\text{Al}_2\text{Sb}_6$ is less than that of $\text{Ca}_5\text{Al}_2\text{Sb}_6$, indicating the larger Seebeck coefficient and the lower conductivity of $\text{Sr}_5\text{Al}_2\text{Sb}_6$. To understand the anisotropy of valence bands of $\text{Sr}_5\text{Al}_2\text{Sb}_6$, we calculated the effective band mass along different directions by:

$$m^* = \hbar \left[\frac{d^2 E(K)}{dk^2} \right]_{E(k)=E_f}^{-1}. \quad (2)$$

The calculated effective mass are $m_{xx}^* = -0.43 m_e$ (along $\Gamma - X$), $m_{yy}^* = -1.04 m_e$ (along $\Gamma - Y$), and $m_{zz}^* = -0.39 m_e$ (along $\Gamma - Z$). Thus, the absolute values of the effective mass along the y -direction is much larger than those along the x - and z -directions, which will induce a larger Seebeck coefficient along the y -direction. The further discussion about Seebeck coefficient will be shown in section C.

The distribution of the density of states (DOS) plays an important role in the study of electronic structure. The calculated partial DOS, total DOS, and the DOS of each type atom of $\text{Sr}_5\text{Al}_2\text{Sb}_6$ and $\text{Ca}_5\text{Al}_2\text{Sb}_6$ are shown in Fig. 4, Fig. 5, and Fig. 6, respectively. As seen in Fig. 4 and Fig. 5, the VBM and CBM of $\text{Ca}_5\text{Al}_2\text{Sb}_6$ are all dominated primarily by Sb atoms. For $\text{Sr}_5\text{Al}_2\text{Sb}_6$, the VBM is also mainly composed of Sb atoms, but the CBM is mainly composed of Sb and Al atoms. According to the DOS of $\text{Sr}_5\text{Al}_2\text{Sb}_6$ shown in Fig. 5 and Fig. 6, the bonding feature between the Al and Sb atoms appears from -4.5 eV to -4

eV and from -3.5 eV to 0 eV, and the corresponding anti-bonding feature does from 0.8 eV to 4.5 eV. For $\text{Ca}_5\text{Al}_2\text{Sb}_6$, Sb-Sb antibonding interaction induces a high DOS peak around -1 eV, as shown in Fig. 6 (b). To understand the difference in Al-Sb bonding between the two compounds, we list the bond distances between Al and Sb atoms in $\text{Sr}_5\text{Al}_2\text{Sb}_6$ and $\text{Ca}_5\text{Al}_2\text{Sb}_6$ in Table II. From this table we can see that the bond distances between the Al and Sb atoms in $\text{Sr}_5\text{Al}_2\text{Sb}_6$ are shorter than that in $\text{Ca}_5\text{Al}_2\text{Sb}_6$, suggesting that the Al-Sb covalent bonding in $\text{Sr}_5\text{Al}_2\text{Sb}_6$ are stronger than that in $\text{Ca}_5\text{Al}_2\text{Sb}_6$. For $\text{Sr}_5\text{Al}_2\text{Sb}_6$, Sb2 atom not only covalently bonds with Al atom, but also with Sb5 atom, and the Sb3 atom in $\text{Ca}_5\text{Al}_2\text{Sb}_6$ also covalently bonds with Al atom and another Sb3 atom. The bond distances between Sb5 and Sb2 in $\text{Sr}_5\text{Al}_2\text{Sb}_6$ is 2.88 Å, while the bond distances between two adjacent Sb3 atoms in $\text{Ca}_5\text{Al}_2\text{Sb}_6$ is 2.84 Å. Hence, the Sb-Sb bonding in $\text{Ca}_5\text{Al}_2\text{Sb}_6$ may be stronger than that in $\text{Sr}_5\text{Al}_2\text{Sb}_6$. The reason for their different band gaps can be also analyzed from their DOS near their CBM. As seen from Fig. 6, for $\text{Sr}_5\text{Al}_2\text{Sb}_6$, all the Sb atoms make contribution to the VBM and CBM. But for the CBM of $\text{Ca}_5\text{Al}_2\text{Sb}_6$, there is a DOS peak of Sb3 atom. Such DOS peak arises from the Sb3-Sb3 antibonding states and leads to a smaller band gap of $\text{Ca}_5\text{Al}_2\text{Sb}_6$ than that of $\text{Sr}_5\text{Al}_2\text{Sb}_6$.

To deeply understand the DOS properties, the band decomposed charge density for the CBM for $\text{Sr}_5\text{Al}_2\text{Sb}_6$ and $\text{Ca}_5\text{Al}_2\text{Sb}_6$ was calculated, and is shown in Fig. 7. From Fig. 7(b), we can see that, for $\text{Ca}_5\text{Al}_2\text{Sb}_6$, the charge density is mainly distributed around the 'rung of ladder', which is composed of the two covalent bonded Sb3. However, there is little charge density around the Sb1 and Sb2 atoms. This is consistent with the DOS peak of the Sb3 atom in $\text{Ca}_5\text{Al}_2\text{Sb}_6$ (Fig. 6). For $\text{Sr}_5\text{Al}_2\text{Sb}_6$, the charge density is mainly distributed near the Sb5 and Sb2 atoms, corresponding to the high DOS of the Sb5 and Sb2 atoms in the conduction band minimum shown in Fig. 6(a). The Sb5 and Sb2 atoms are covalently bonded, as well as the Sb3-Sb3 bonds in $\text{Ca}_5\text{Al}_2\text{Sb}_6$. However, the DOS of the Sb5 and Sb2 atoms in $\text{Sr}_5\text{Al}_2\text{Sb}_6$ are much lower than the DOS of Sb3 atom in $\text{Ca}_5\text{Al}_2\text{Sb}_6$. The possible reason is that the stronger Al-Sb covalent bond in $\text{Sr}_5\text{Al}_2\text{Sb}_6$ attracts more electrons and thus decreases the electrons of the Sb-Sb covalent bonds in $\text{Sr}_5\text{Al}_2\text{Sb}_6$. The bond distances between Sb5 and Sb2 in $\text{Sr}_5\text{Al}_2\text{Sb}_6$ and that between adjacent Sb3 atoms in $\text{Ca}_5\text{Al}_2\text{Sb}_6$ demonstrate this idea.

C. Transport properties

A promising thermoelectric material must have a large Seebeck coefficient, a high electrical conductivity, and a low thermal conductivity. As previously mentioned, $\text{Sr}_5\text{Al}_2\text{Sb}_6$ has a low thermal conductivity.[6] Thus, to enhance thermoelectric properties of $\text{Sr}_5\text{Al}_2\text{Sb}_6$, it is an effective method to increase its thermoelectric power factor ($S^2\sigma$). However, Seebeck coefficient and electrical conductivity have strongly coupled nature *via* carrier concentration. Therefore, it is valuable to find an optimal carrier concentration for maximizing ZT of $\text{Sr}_5\text{Al}_2\text{Sb}_6$. In this work, we simulated the doping effects and calculated the transport properties of $\text{Sr}_5\text{Al}_2\text{Sb}_6$ as a function of carrier concentration from $1 \times 10^{19} \text{ cm}^{-3}$ to $5 \times 10^{21} \text{ cm}^{-3}$ at 500 K and 800 K with the semiclassical Boltzmann theory without considering special dopant type, as shown Fig. 8. For comparison, the transport properties of $\text{Ca}_5\text{Al}_2\text{Sb}_6$ at 800 K were also calculated with the same method, and is also shown in Fig. 8. From Fig. 8, we can see that $\text{Sr}_5\text{Al}_2\text{Sb}_6$ has larger Seebeck coefficient and lower electrical conductivity than that of $\text{Ca}_5\text{Al}_2\text{Sb}_6$, corresponding to the previously mentioned in section B.

From Fig. 8(d), we can see that the Seebeck coefficient of $\text{Sr}_5\text{Al}_2\text{Sb}_6$ is inversely proportional to carrier concentration. For *n*-type $\text{Sr}_5\text{Al}_2\text{Sb}_6$ at 800 K, there is an obvious bipolar effect when the carrier concentration is below $7.4 \times 10^{19} \text{ cm}^{-3}$. It is known that the bipolar effect is unfavorable to thermoelectric performance and is the consequence of the combined action of two types of carriers which participate in transportation. Thus, to obtain large Seebeck coefficient, it is necessary to find ways to reduce the bipolar effect. As 500 K, the bipolar effect almost disappears. It is also found that *n*-type $\text{Sr}_5\text{Al}_2\text{Sb}_6$ has larger Seebeck coefficients than those of *p*-type one at the same carrier concentration, and the anisotropy of the *p*-type one is stronger. This can be explained by the DOS effective mass. For a given Fermi energy, the Seebeck coefficient is proportional to the DOS effective mass.[21] The DOS effective mass can be written as:

$$m_{DOS}^* = (m_{xx}^* m_{yy}^* m_{zz}^*)^{1/3} N_v^{2/3}, \quad (3)$$

where N_v is the band degeneracy, m_{xx}^* , m_{yy}^* , and m_{zz}^* are the band effective mass components along the three perpendicular directions xx, yy, and zz, respectively. From the calculated band structure, shown in Fig. 3, we can see that the dispersion of the CBM along different directions are small, indicating the large DOS effective mass and corresponding to larger Seebeck coefficients for *n*-type $\text{Sr}_5\text{Al}_2\text{Sb}_6$. In contrast, the VBM has a stronger dispersion.

Thus, due to the relatively small dispersion of the CBM, the Seebeck coefficient of n -type $\text{Sr}_5\text{Al}_2\text{Sb}_6$ should be larger than that of p -type one. The anisotropy of the Seebeck coefficient in p -type $\text{Sr}_5\text{Al}_2\text{Sb}_6$ can be explained by the different effective mass along different directions. Our calculated effective mass along the y -direction is much larger than those along other two directions. Consequently, its Seebeck coefficient along the y direction should be larger than those along other two directions.

The electrical conductivity of $\text{Sr}_5\text{Al}_2\text{Sb}_6$ as a function of carrier concentration was calculated and plotted in Fig. 8(e). The relationship between electrical conductivity and carrier concentration is shown as:[22]

$$\sigma = ne\mu = \frac{1}{\rho}, \quad (4)$$

$$\mu \propto \frac{1}{m^{*5/2}}, \quad (5)$$

here, m^* is the band effective mass of a single valley. From Eq. 4, we can see that the electrical conductivity is proportional to carrier concentration, and this explains the change of σ with the increasing of n in Fig. 8(e). However, the calculated $\frac{\sigma}{\tau}$ includes scattering rate τ^{-1} . Here we used semi-empirical method to take off the τ and get the value of σ . By comparing the experimental σ and our calculated $\frac{\sigma}{\tau}$ at same temperature and carrier concentration, we can obtain τ . The experimental data of electrical conductivity and carrier concentration are taken from Ref. [6]. As shown in Ref. [6], for $\text{Sr}_5\text{Al}_2\text{Sb}_6$, at 800 K, $\sigma = 943 \Omega^{-1} \text{m}^{-1}$ and $n = 1.2 \times 10^{19} \text{cm}^{-3}$. Our calculated value $\frac{\sigma}{\tau}$ at the same carrier concentration and temperature is $7.6 \times 10^{16} \Omega^{-1} \text{m}^{-1} \text{s}^{-1}$. Thus, we can get $\tau = 1.24 \times 10^{-14} \text{s}$ for $\text{Sr}_5\text{Al}_2\text{Sb}_6$ at 800 K. For doping dependence, there is a standard electron-phonon form, $\tau \propto n^{-1/3}$, and within certain regime, there is an approximate electron-phonon T dependence, $\sigma \propto T^{-1}$. [23] Thus, for $\text{Sr}_5\text{Al}_2\text{Sb}_6$, this yields

$$\tau = 2.5 \times 10^{-5} T^{-1} n^{-1/3} \quad (6)$$

with τ in s, T in K, and n in cm^{-3} . For $T = 800 \text{K}$, Eq. 5 can be written as $\tau = 2.8 \times 10^{-8} n^{-1/3}$. As shown in Fig. 8(e), the electrical conductivities of p -type $\text{Sr}_5\text{Al}_2\text{Sb}_6$ are higher than that of n -type one, apparently. This may be explained by the relatively large band effective mass of its CBM. According to Eq. 4 and Eq. 5, the σ is inversely proportional to m^* , the stronger dispersion, the smaller effective mass of a band. From the calculated band structure shown in Fig. 3, we can see that the dispersion of the valence band is stronger than

that of conduction band obviously, therefore the electrical conductivity of *p*-type $\text{Sr}_5\text{Al}_2\text{Sb}_6$ should be higher. For *p*-type $\text{Sr}_5\text{Al}_2\text{Sb}_6$, the electrical conductivity along the *y* direction decreases at first and then increases, due to the change of band effective mass with the change of doping degree. As known that the Fermi level will shift down with the increasing of *p*-type doping degree. From the band structures shown in Fig. 3 we can see that, for $\text{Sr}_5\text{Al}_2\text{Sb}_6$, the band effective mass along Γ -Y is larger than those along other two directions at VBM, as previously mentioned. Thus, the electrical conductivity of lightly doped *p*-type $\text{Sr}_5\text{Al}_2\text{Sb}_6$ along the *y* direction is lower than other two directions. However, when the carrier concentration is $1.26 \times 10^{21} \text{ cm}^{-3}$, the doping degree is heavy, and the Fermi level shifts down. When the Fermi level shifts around -0.25 eV, the calculated band effective mass are: $m_{xx}^* = -3.67 m_e$, $m_{yy}^* = -0.14 m_e$, and $m_{zz}^* = 10.36 m_e$. Thus, the electrical conductivity of *p*-type $\text{Sr}_5\text{Al}_2\text{Sb}_6$ along the *y* direction becomes highest. For $\text{Ca}_5\text{Al}_2\text{Sb}_6$, the calculated band effective mass at VBM are: $m_{xx}^* = -2.17 m_e$, $m_{yy}^* = -0.28 m_e$, and $m_{zz}^* = -0.22 m_e$, leading to the high electrical conductivity along the *z* direction. With the shift down of the Fermi level, the dispersion of the bands along Γ -Z is always the strongest, corresponding to the high electrical conductivity of *p*-type $\text{Ca}_5\text{Al}_2\text{Sb}_6$ along the *z* direction.

The optimal electronic performance of a thermoelectric semiconductor depends primarily on the weighted mobility μ_w , [22, 24, 25]

$$\mu_w = \mu(m_{DOS}^*/m_e), \quad (7)$$

here m_e is the electron mass. Combining Eq. 2, Eq. 5, and Eq. 7, we can get:

$$\mu_w \propto \frac{N_v}{m^{*5/2}m_e}. \quad (8)$$

Thus, the weighted mobility is proportional to the band degeneracy and inversely proportional to the band effective mass. Therefore, the band effective mass and band degeneracy should determine the thermoelectric performance. From the band structures shown in Fig. 3 we can see that, for $\text{Sr}_5\text{Al}_2\text{Sb}_6$, the band degeneracy of the VBM along different directions are all 1, but it is different near -0.25 eV. The band degeneracy along Γ -Y is 2, and along Γ -X and Γ -Z directions are still 1 near -0.25 eV. Considering the band effective mass as discussed above, we can conclude that *p*-type $\text{Sr}_5\text{Al}_2\text{Sb}_6$ has promising thermoelectric properties along the *y* direction. For $\text{Ca}_5\text{Al}_2\text{Sb}_6$, the band degeneracy along different directions are same with the shift of the Fermi level from VBM to -0.25 eV. Moreover, the band effective mass

along Γ -Z is always smaller than those along other two directions. Thus, p -type $\text{Ca}_5\text{Al}_2\text{Sb}_6$ may have promising thermoelectric properties along the z direction.

To find an optimal carrier concentration for achieving a high ZT value, we need to study the dependence of ZT on carrier concentration. However, there is no experimental results about the anisotropy of lattice thermal conductivity and the anisotropy of relaxation time for carriers. Thus, in the current study, we do not consider the anisotropy on thermal conductivity and relaxation time, and we used the experimental thermal conductivity to roughly estimate the ZT values along different directions as a function of carrier concentration. For this reason, our predicted ZT value may have a slight difference from the experimental ones. Moreover, previous experimentally synthesized samples of $\text{Sr}_5\text{Al}_2\text{Sb}_6$ and $\text{Ca}_5\text{Al}_2\text{Sb}_6$ are not crystal and are isotropic. Our predicted ZT values are anisotropic along different directions. Our predicted ZT results may be helpful to understand well the ZT properties of crystalline samples and find the direction with highest thermoelectric performance. Fig. 8(f) shows the ZT value of $\text{Sr}_5\text{Al}_2\text{Sb}_6$, here the thermal conductivity κ was used as experimental value 0.53 W/mK.[6] From Fig. 8 we can see that p -type $\text{Sr}_5\text{Al}_2\text{Sb}_6$ along the y direction has larger Seebeck coefficients and higher conductivities than those along the x and z directions. Consequently, at 800 K, the highest ZT value of p -type $\text{Sr}_5\text{Al}_2\text{Sb}_6$ appears in the y direction and is 1.01 with a carrier concentration of $1.26 \times 10^{21} \text{ cm}^{-3}$. For $\text{Ca}_5\text{Al}_2\text{Sb}_6$ at 800 K, the highest ZT value of $\text{Ca}_5\text{Al}_2\text{Sb}_6$ is 1.37 and appears in p -type doping along the z direction with the carrier concentration of $6.07 \times 10^{19} \text{ cm}^{-3}$. The reason is that the effective mass of top of valence bands along Γ -Z in $\text{Ca}_5\text{Al}_2\text{Sb}_6$ ($-0.22 m_e$) is very small, which leads to the high electrical conductivity of $\text{Ca}_5\text{Al}_2\text{Sb}_6$ along this direction. For n -type $\text{Sr}_5\text{Al}_2\text{Sb}_6$, their ZT values profit from their relatively high Seebeck coefficient, leading to the highest ZT value of 0.70 along the y direction, corresponding to the carrier concentration of $1.31 \times 10^{21} \text{ cm}^{-3}$. From Fig. 8(f), we can see that p -type $\text{Sr}_5\text{Al}_2\text{Sb}_6$ may have larger ZT values than n -type one. Considering the influence of Seebeck coefficient and electrical conductivity on ZT value, we can see that the high Seebeck coefficient induces the high ZT value of the p -type $\text{Sr}_5\text{Al}_2\text{Sb}_6$.

IV. CONCLUSION

Summary, the stability, electronic structure, and transport properties of $\text{Sr}_5\text{Al}_2\text{Sb}_6$ and $\text{Ca}_5\text{Al}_2\text{Sb}_6$ were studied by the first-principles calculations and the semiclassical Boltzmann theory. The formation energies of several doped $\text{Sr}_5\text{Al}_2\text{Sb}_6$ were calculated. The result shows that the formation energies of Na-doped at the Sr site and Mn-doped at the Al site are negative. Thus, we propose that the doped $\text{Sr}_5\text{Al}_2\text{Sb}_6$ with Na^{1+} and Mn^{2+} are easier to be realized and have higher hole concentrations, corresponding to p -type $\text{Sr}_5\text{Al}_2\text{Sb}_6$. The high positive formation energy of Zn-doped $\text{Sr}_5\text{Al}_2\text{Sb}_6$ means that it is difficult to achieve high carrier concentration by Zn-doping, which agrees well with the low carrier concentration of Zn-doped $\text{Sr}_5\text{Al}_2\text{Sb}_6$ determined by experiment work. The simulated doping effect on $\text{Sr}_5\text{Al}_2\text{Sb}_6$ shows that $\text{Sr}_5\text{Al}_2\text{Sb}_6$ has a higher Seebeck coefficient and a lower electrical conductivity than that of $\text{Ca}_5\text{Al}_2\text{Sb}_6$. For $\text{Sr}_5\text{Al}_2\text{Sb}_6$, the high Seebeck coefficient along the y direction mainly comes from the large hole effective mass along Γ -Y. For $\text{Ca}_5\text{Al}_2\text{Sb}_6$, the always small hole effective mass along the z direction with increasing doping degree induces a high electrical conductivity along the z direction, which is helpful for achieving high thermoelectric performance along this direction. The different band gaps between the two compounds result from their different Sb-Sb interactions.

V. ACKNOWLEDGMENTS

This research was sponsored by the National Natural Science Foundation of China (grant Nos. U1204112, 51371076), and the Program for Innovative Research Team (in Science and Technology) in University of Henan Province (grant No. 13IRTSTHN01 7).

-
- [1] G. Mahan, B. Sales, and J. Sharp, *Phys. Today* **50**, 42 (2008).
 - [2] G. J. Snyder and E. S. Toberer, *Nat. Mater.* **7**, 105 (2008).
 - [3] S. M. Kauzlarich, *Chemistry, structure, and bonding of Zintl phases and ions* (VCH New York, 1996).
 - [4] E. S. Toberer, A. F. May, and G. J. Snyder, *Chem. Mater.* **22**, 624 (2009).
 - [5] S. M. Kauzlarich, S. R. Brown, and G. J. Snyder, *Dalton Trans.* **21**, 2099 (2007).

- [6] A. Zevalkink, Y. Takagiwa, K. Kitahara, K. Kimura, and G. J. Snyder, *Dalton Trans.* **43**, 4720 (2014).
- [7] E. S. Toberer, A. Zevalkink, N. Crisosto, and G. J. Snyder, *Adv. Funct. Mater.* **20**, 4375 (2010).
- [8] A. Zevalkink, E. S. Toberer, T. Bleith, E. Flage-Larsen, and G. J. Snyder, *J. Appl. Phys.* **110**, 013721 (2011).
- [9] Y. L. Yan and Y. X. Wang, *J. Mater. Chem.* **21**, 12497 (2011).
- [10] S. I. Johnson, A. Zevalkink, and G. J. Snyder, *J. Mater. Chem. A* **1**, 4244 (2013).
- [11] A. Zevalkink, J. Swallow, and G. J. Snyder, *Dalton Trans.* **42**, 9713 (2013).
- [12] A. Zevalkink, E. S. Toberer, W. G. Zeier, E. Flage-Larsen, and G. J. Snyder, *Energy Environ. Sci.* **4**, 510 (2011).
- [13] G. Kresse and J. Hafner, *Phys. Rev. B* **47**, 558 (1993).
- [14] G. Kresse and J. Hafner, *J. Phys.: Condens. Matter* **6**, 8245 (1994).
- [15] L. Nordstrom and D. J. Singh, *Planewaves, Pseudopotentials, and the LAPW method* (Springer, 2006).
- [16] D. Koelling and B. Harmon, *J. Phys. C: Solid State Phys.* **10**, 3107 (1977).
- [17] P. Hohenberg and W. Kohn, *Phys. Rev.* **136**, B864 (1964).
- [18] P. Blaha, K. Schwarz, G. Madsen, D. Kvasnicka, and J. Luitz, Schwarz (Vienna University of Technology, Austria, 2001) (2001).
- [19] G. K. Madsen and D. J. Singh, *Comput. Phys. Commun.* **175**, 67 (2006).
- [20] A. Zevalkink, J. Swallow, and G. J. Snyder, *J. Electron. Mater.* **41**, 813 (2012).
- [21] M. Cutler, J. Leavy, and R. Fitzpatrick, *Phys. Rev.* **133**, A1143 (1964).
- [22] H. J. Goldsmid, (1964).
- [23] K. P. Ong, D. J. Singh, and P. Wu, *Phys. Rev. B* **83**, 115110 (2011).
- [24] G. Mahan, Academic Press, New York **51**, 11 (1998).
- [25] G. Slack, "New materials and performance limits for thermoelectric cooling in circ. handbook of thermoelectric," (1995).

TABLE I. The number of the crystallographically unique Sr, Al, and Sb atoms per primitive cell of $\text{Sr}_5\text{Al}_2\text{Sb}_6$.

Atom	Sr1	Sr2	Sr3	Sb1	Sb2
Number	8	8	4	8	4
Atom	Sb3	Sb4	Sb5	Al1	Al2
Number	4	4	4	4	4

TABLE II. The bond distances (\AA) between Al and Sb in $\text{Ca}_5\text{Al}_2\text{Sb}_6$ and $\text{Sr}_5\text{Al}_2\text{Sb}_6$.

Material	Bond type and length		
$\text{Ca}_5\text{Al}_2\text{Sb}_6$	Al-Sb1	Al-Sb2	Al-Sb3
	2.74	2.70	2.83
$\text{Sr}_5\text{Al}_2\text{Sb}_6$	Al1-Sb1	Al1-Sb2	Al1-Sb3
	2.66	2.73	2.66
	Al2-Sb1	Al2-Sb3	Al2-Sb4
	2.69	2.76	2.65

TABLE III. The calculated formation energies of $\text{Sr}_5\text{Al}_2\text{Sb}_6$ by using B atoms to replace A atoms.

Doping type	A = Sr, B = Na	A = Sr, B = K	A = Al, B = Zn	A = Al, B = Mn
$\text{Sr}_5\text{Al}_2\text{Sb}_6$	-3.32	5.20	15.80	-6.58

FIGURE CAPTIONS

- : Fig. 1. The optimized orthorhombic structure of $\text{Sr}_5\text{Al}_2\text{Sb}_6$ with space group of $Pnma$, forming by non-linear and oscillating chains extend infinitely along the a axis. Sr, Al, and Sb atoms are shown in small green, red, and blue spheres, respectively. The edge sharing Sb1 and corner sharing Sb3 are all covalently bonded with two Al atoms, and the Sb2 atom is covalently bonded with Al and Sb5 atoms, and Sb5 and Sb4 are covalently bonded with Sb2 and Al atoms, respectively.
- : Fig. 2. The orthorhombic structure of $\text{Ca}_5\text{Al}_2\text{Sb}_6$ with space group of $Pbam$, formed by ladder-like chains extend infinitely along the c axis. Ca, Al, and Sb atoms are shown in big blue sphere, small red, and small blue spheres, respectively. The corner sharing Sb1 atom is covalently bonded with two Al atoms, and the Sb3 atom is covalently bonded with another Sb3 atom, and the Sb1 atom is covalently bonded with Al atom.
- : Fig. 3. Band structure of $\text{Sr}_5\text{Al}_2\text{Sb}_6$ and $\text{Ca}_5\text{Al}_2\text{Sb}_6$, the high symmetry k points Γ , X, S, R, U, Z, Y, and T in the figure represent the points (0, 0, 0), (0.5, 0, 0), (0.5, 0.5, 0), (0.5, 0.5, 0.5), (0.5, 0, 0.5), (0, 0, 0.5), (0, 0.5, 0), and (0, 0.5, 0.5), respectively.
- : Fig. 4. Partial DOS for $\text{Sr}_5\text{Al}_2\text{Sb}_6$ and $\text{Ca}_5\text{Al}_2\text{Sb}_6$. The Fermi level is set at zero.
- : Fig. 5. Total DOS for $\text{Sr}_5\text{Al}_2\text{Sb}_6$ and $\text{Ca}_5\text{Al}_2\text{Sb}_6$. The Fermi level is set at zero.
- : Fig. 6. DOS of Al and Sb atoms for $\text{Sr}_5\text{Al}_2\text{Sb}_6$ and $\text{Ca}_5\text{Al}_2\text{Sb}_6$. The Fermi level is set at zero.
- : Fig. 7. Band decomposed charge density of conduction band minimum for $\text{Sr}_5\text{Al}_2\text{Sb}_6$ (a) and $\text{Ca}_5\text{Al}_2\text{Sb}_6$ (b). The isosurface value is set as 0.001.
- : Fig. 8. Calculated transport properties of $\text{Sr}_5\text{Al}_2\text{Sb}_6$ and $\text{Ca}_5\text{Al}_2\text{Sb}_6$ as a function of carrier concentration from $1 \times 10^{19} \text{ cm}^{-3}$ to $5 \times 10^{21} \text{ cm}^{-3}$.

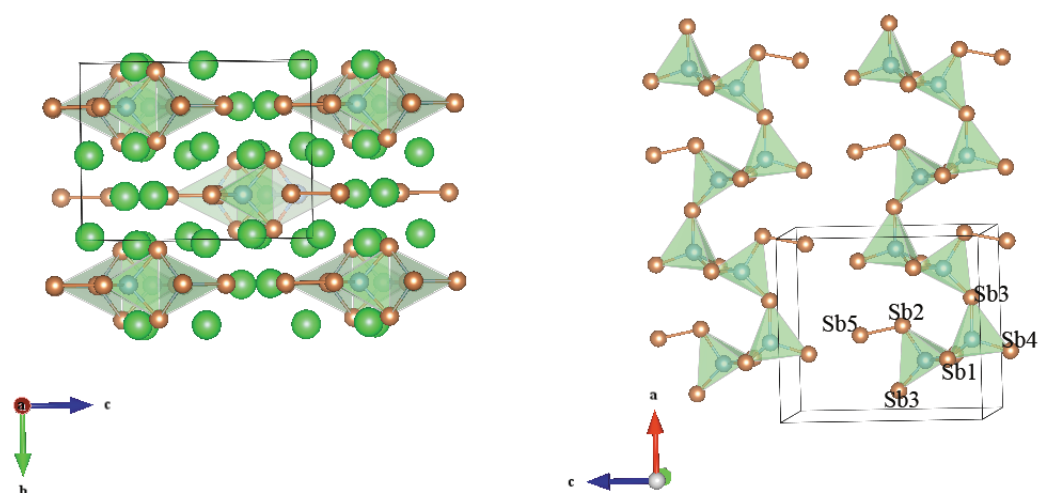


FIG. 1. The optimized orthorhombic structure of $\text{Sr}_5\text{Al}_2\text{Sb}_6$ with space group of $Pnma$, forming by non-linear and oscillating chains extend infinitely along the a axis. Sr, Al, and Sb atoms are shown in small green, red, and blue spheres, respectively. The edge sharing Sb1 and corner sharing Sb3 are all covalently bonded with two Al atoms, and the Sb2 atom is covalently bonded with Al and Sb5 atoms, and Sb5 and Sb4 are covalently bonded with Sb2 and Al atoms, respectively.

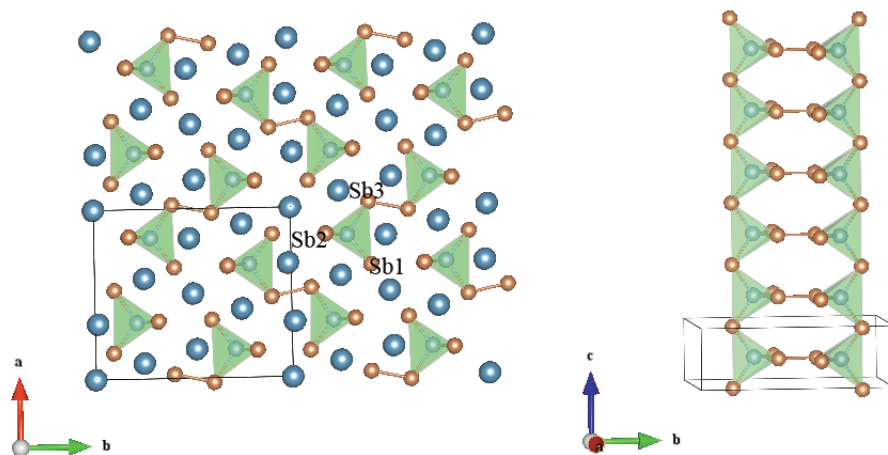


FIG. 2. The orthorhombic structure of $\text{Ca}_5\text{Al}_2\text{Sb}_6$ with space group of $Pbam$, forming by ladder-like chains extend infinitely along the c -axis. Ca, Al and Sb atoms are shown in big blue sphere, small red, and small blue spheres, respectively. The corner sharing Sb1 atom is covalently bonded with two Al atoms, and the Sb3 atom is covalently bonded with another Sb3 atom, and the Sb1 atom is covalently bonded with Al atom.

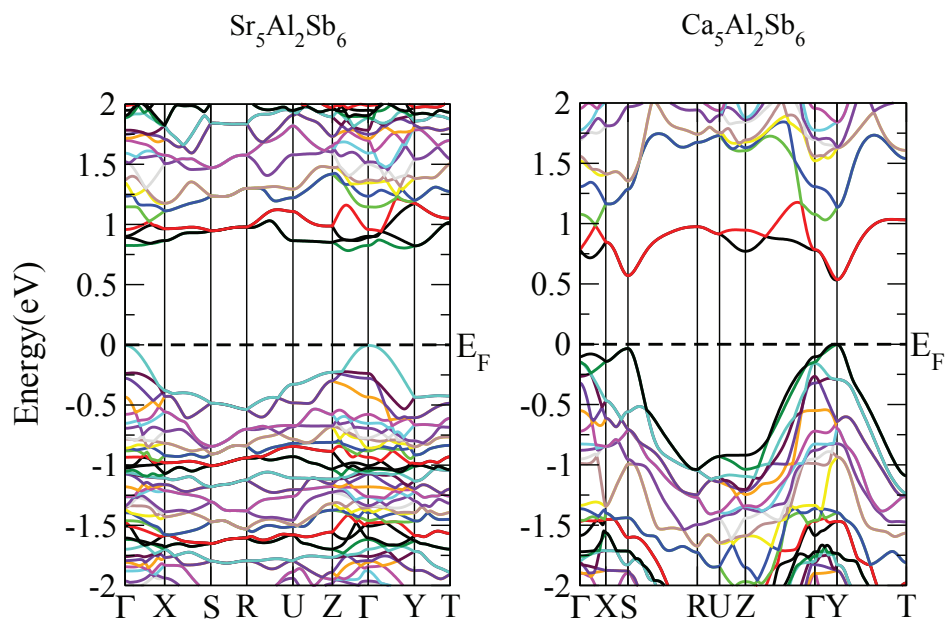


FIG. 3. Band structure of $\text{Sr}_5\text{Al}_2\text{Sb}_6$ and $\text{Ca}_5\text{Al}_2\text{Sb}_6$, the high symmetry k points Γ , X, S, R, U, Z, Y, and T in the figure represent the points (0, 0, 0), (0.5, 0, 0), (0.5, 0.5, 0), (0.5, 0.5, 0.5), (0.5, 0, 0.5), (0, 0, 0.5), (0, 0.5, 0), and (0, 0.5, 0.5), respectively.

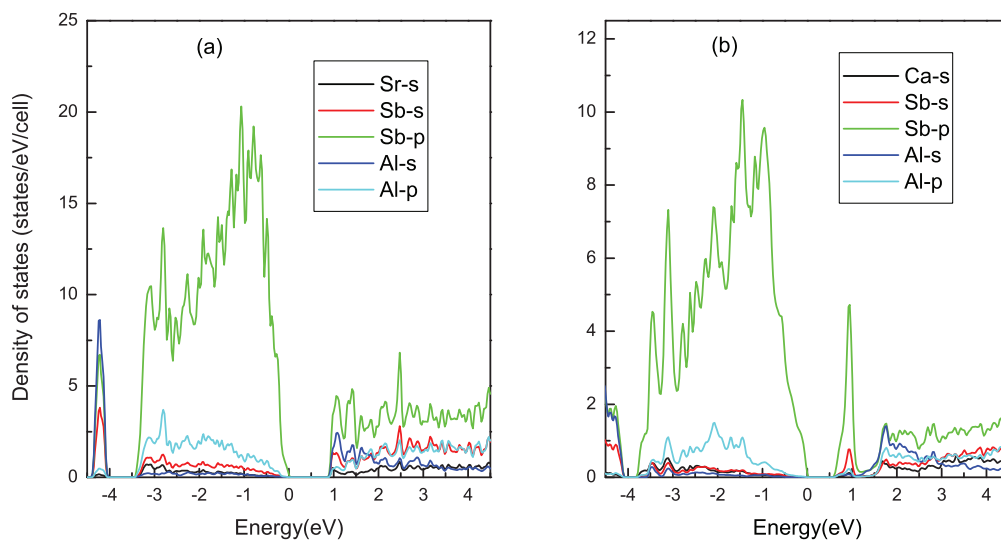


FIG. 4. Partial DOS for $\text{Sr}_5\text{Al}_2\text{Sb}_6$ and $\text{Ca}_5\text{Al}_2\text{Sb}_6$. The Fermi level is set at zero.

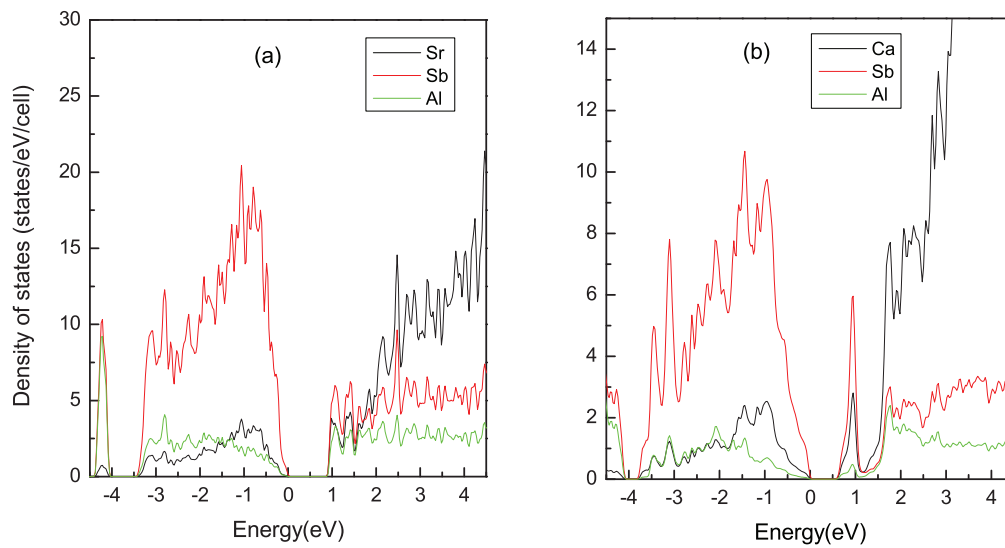


FIG. 5. Total DOS for $\text{Sr}_5\text{Al}_2\text{Sb}_6$ and $\text{Ca}_5\text{Al}_2\text{Sb}_6$. The Fermi level is set at zero.

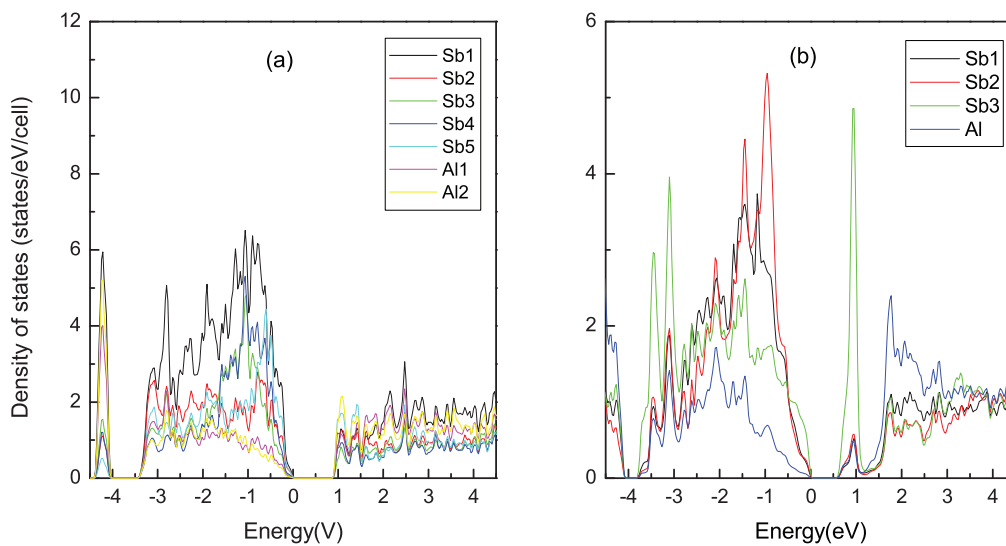


FIG. 6. DOS of Al and Sb atoms for $\text{Sr}_5\text{Al}_2\text{Sb}_6$ and $\text{Ca}_5\text{Al}_2\text{Sb}_6$. The Fermi level is set at zero.

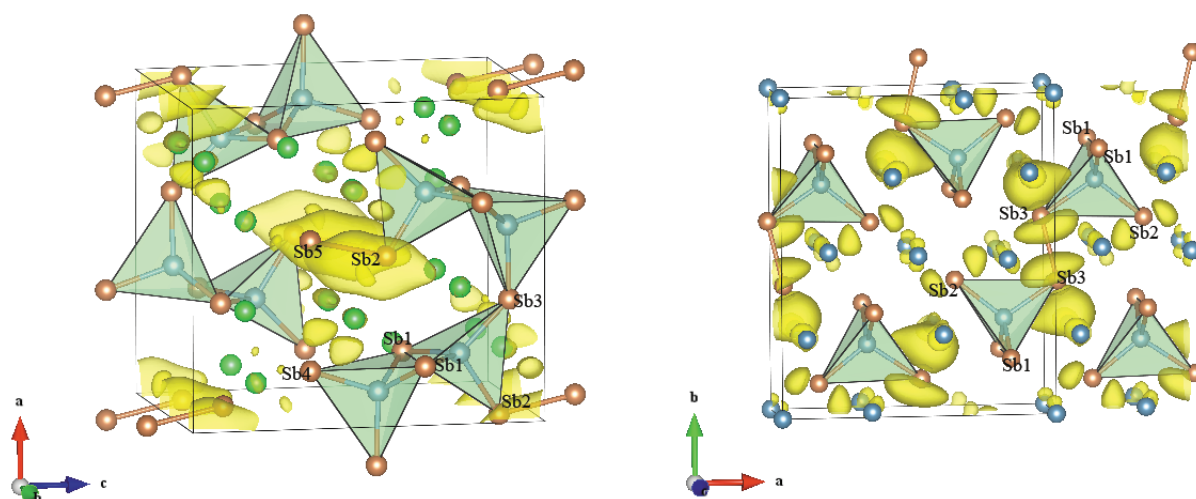


FIG. 7. Band decomposed charge density of conduction band minimum for $\text{Sr}_5\text{Al}_2\text{Sb}_6$ (a) and $\text{Ca}_5\text{Al}_2\text{Sb}_6$ (b). The isosurface value is set as 0.001.

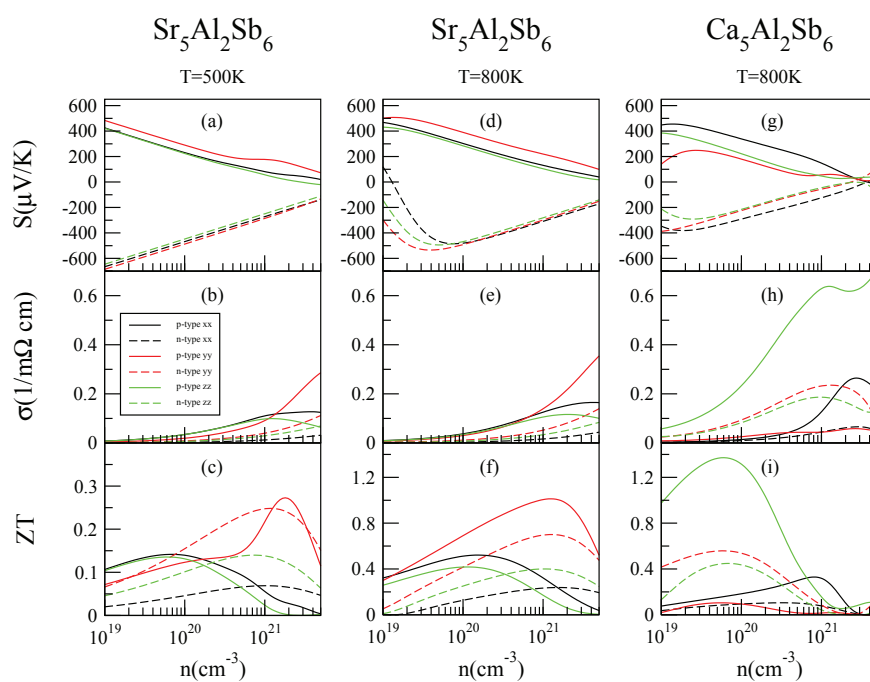


FIG. 8. Calculated transport properties of $\text{Sr}_5\text{Al}_2\text{Sb}_6$ and $\text{Ca}_5\text{Al}_2\text{Sb}_6$ as a function of carrier concentration from $1 \times 10^{19} \text{ cm}^{-3}$ to $5 \times 10^{21} \text{ cm}^{-3}$.